frontiers | Frontiers in Immunology

TYPE Original Research
PUBLISHED 15 December 2022
DOI 10.3389/fimmu.2022.1034336

OPEN ACCESS

EDITED BY
Deborah K. Dunn-Walters,
University of Surrey, United Kingdom

REVIEWED BY
Laura Mandik-Nayak,
Lankenau Institute for Medical Research, United States
Muhammad Shahnawaz Soyfoo,
Université libre de Bruxelles, Belgium

*CORRESPONDENCE
Jill M. Kramer
jkramer@buffalo.edu

†PRESENT ADDRESS
Jeremy Kiripolsky,
Thermo Fischer Scientific, Grand Island, NY, United States

SPECIALTY SECTION
This article was submitted to B Cell Biology, a section of the journal Frontiers in Immunology

RECEIVED 01 September 2022
ACCEPTED 30 November 2022
PUBLISHED 15 December 2022

CITATION
Punnanitinont A, Kasperek EM, Kiripolsky J, Zhu C, Miecznikowski JC and Kramer JM (2022) TLR7 agonism accelerates disease in a mouse model of primary Sjögren's syndrome and drives expansion of T-bet$^+$ B cells. *Front. Immunol.* 13:1034336. doi: 10.3389/fimmu.2022.1034336

TLR7 agonism accelerates disease in a mouse model of primary Sjögren's syndrome and drives expansion of T-bet$^+$ B cells

Achamaporn Punnanitinont[1], Eileen M. Kasperek[1], Jeremy Kiripolsky[1†], Chengsong Zhu[2], Jeffrey C. Miecznikowski[3] and Jill M. Kramer[1*]

[1]Department of Oral Biology, School of Dental Medicine, The University at Buffalo, State University of New York, Buffalo, NY, United States, [2]Department of Immunology, Microarray & Immune Phenotyping Core Facility, University of Texas Southwestern Medical Center, Dallas, TX, United States, [3]Department of Biostatistics, School of Public Health and Health Professions, The University at Buffalo, State University of New York, Buffalo, NY, United States

Primary Sjögren's syndrome (pSS) is a systemic autoimmune disease characterized by chronic inflammation of exocrine tissue, resulting in loss of tears and saliva. Patients also experience many extra-glandular disease manifestations. Treatment for pSS is palliative, and there are currently no treatments available that target disease etiology. Previous studies in our lab demonstrated that MyD88 is crucial for pSS pathogenesis in the NOD.B10Sn-*H2*^{b} (NOD.B10) pSS mouse model, although the way in which MyD88-dependent pathways become activated in disease remains unknown. Based on its importance in other autoimmune diseases, we hypothesized that TLR7 activation accelerates pSS pathogenesis. We administered the TLR7 agonist Imiquimod (Imq) or sham treatment to pre-disease NOD.B10 females for 6 weeks. Parallel experiments were performed in age and sex-matched C57BL/10 controls. Imq-treated pSS animals exhibited cervical lymphadenopathy, splenomegaly, and expansion of TLR7-expressing B cells. Robust lymphocytic infiltration of exocrine tissues, kidney and lung was observed in pSS mice following treatment with Imq. TLR7 agonism also induced salivary hypofunction in pSS mice, which is a hallmark of disease. Anti-nuclear autoantibodies, including Ro (SSA) and La (SSB) were increased in pSS mice following Imq administration. Cervical lymph nodes from Imq-treated NOD.B10 animals demonstrated an increase in the percentage of activated/memory CD4+ T cells. Finally, T-bet$^+$ B cells were expanded in the spleens of Imq-treated pSS mice. Thus, activation of TLR7 accelerates local and systemic disease and promotes expansion of T-bet-expressing B cells in pSS.

KEYWORDS

autoantibodies, NOD.B10, autoimmunity, age-associated B cells, ABC, sialadenitis

1 Introduction

Primary Sjögren's syndrome (pSS, also referred to as Sjögren's disease) is an autoimmune disease that primarily affects women. Patients with pSS experience many debilitating disease manifestations, including salivary hypofunction, diminished tear production, interstitial lung disease and nephritis (1). In addition, several hematopoietic abnormalities are noted, such as hypergammaglobulinemia and hypocomplementemia (2, 3) and pSS patients are at increased risk of B cell lymphoma development (4). Primary SS is incurable at present, although clinical trials are ongoing to discover effective therapeutics (5). Previous studies from our group and others highlight the importance of MyD88-mediated signaling cascades in specific disease manifestations (6–8), although the receptor-ligand interactions that culminate in MyD88-dependent disease sequelae remain incompletely understood. Indeed, additional studies are needed to define the molecular networks that contribute to disease initiation and persistence.

Both TLR and IL-1R family members drive MyD88-dependent inflammation, and TLR7 is a MyD88-dependent endosomal TLR that has been shown to be of critical importance in several autoimmune diseases (9–11), most notably Systemic Lupus Erythematosus (SLE) or lupus (12). Since SLE shares overlapping clinical and molecular features with pSS (13–16), we hypothesized that activation of TLR7 accelerates disease in a pSS mouse model.

Although TLR7 is expressed by diverse cells types, there is considerable evidence that the activation of TLR7-expressing B cells, in particular, is a central disease mechanism that drives SLE in mice and humans (17–20). TLR7 plays an integral role in host defense, as it elicits a protective response upon recognition of single-stranded viral RNA (21). Seminal studies revealed that self-derived ligands also activate TLR7, including RNA-associated immune complexes and U11 small nuclear RNA (U11snRNA), and this ability to recognize self-derived moieties underlies its pivotal role in autoimmunity (22–24).

Although there is compelling evidence that TLR7 is integral to lupus pathogenesis, there is a relative paucity of studies examining this TLR in pSS. Indeed, TLR7 activation is implicated in pSS patients, but little is known regarding its role in disease. Studies in pSS patients reveal TLR7 is expressed and elevated in salivary gland epithelial cells, minor salivary glands, and in parotid tissues from pSS patients (25–28). Additionally, TLR7 is dysregulated in the immune compartment, as levels are increased in PBMCs, B cells, and $CD14^+$ monocytes from pSS patients (26, 28–31). Treatment of pSS B cells with a TLR7 agonist (CL264) caused elevated IFNα secretion as compared to B cells derived from healthy controls (30). Moreover, stimulation of TLR7 in pSS patient-derived naïve B cells using Imiquimod (Imq) resulted in increased plasma cell differentiation and class switching compared to B cells from healthy controls (32). Lastly, alterations in TLR7 signaling were identified in PBMCs from pSS patients using phosphorylation profiling (33).

Data from mouse models also provide corroborating evidence that TLR7 agonism mediates organ-specific disease (11, 34, 35). Studies in *TLR8-/-* animals revealed that these mice develop lupus and SS concomitantly, as sialadenitis, autoantibody production, immune complex deposition, salivary cytokine production, glomerulonephritis, and lung inflammation were observed (34, 36). These disease manifestations were dependent on TLR7, as disease was abrogated in mice lacking both TLR7 and TLR8 (34, 36). While these studies provide compelling evidence that TLR7 mediates SS, it is important to note that SS and lupus share overlapping disease features and so it is difficult to examine disease characteristics that result from SS specifically in the background of another autoimmune disease (15, 16). Further work in the NOD/ShiLtJ model revealed that TLR7 is required for lacrimal gland inflammation that is characteristic of SS (11). It is also challenging to assess SS-specific disease manifestations in the NOD/ShiLtJ mouse model, however, as these animals develop SS and type 1 diabetes (T1D), and hyperglycemia often accompanies T1D in this strain. Recent work revealed that hyperglycemia seen in the context of T1D influences salivary disease manifestations previously thought to be specific for SS (37, 38). Thus, given the potential of other autoimmune conditions to influence or confound interpretation of SS-related disease manifestations, studies are needed in pSS models to examine how TLR7 activation mediates SS-specific pathology.

To this end, we treated pre-disease stage (6-week-old) NOD.B10Sn-$H2^b$ (NOD.B10) pSS females with the TLR7 agonist Imiquimod (Imq) for 6 weeks, euthanized the animals, and evaluated local and systemic disease. Of note, we used a well-characterized pSS mouse model that develops clinical stage disease at 26 weeks of age. The use of pre-disease mice allowed us to determine if TLR7 activation accelerates disease, as animals normally display negligible signs of disease at 12 weeks of age (39). We performed parallel studies in age and sex-matched C57BL/10 (BL/10) healthy controls to assess whether the changes induced by Imq treatment were more robust in the pSS model. Strikingly, NOD.B10 mice exhibited cervical lymphadenopathy and splenomegaly following topical Imq treatment. Additionally, the percentage of TLR7-expressing cervical lymph node (cLN) B cells was expanded in NOD.B10 mice that received the TLR7 agonist. TLR7 agonism promoted exocrine-gland inflammation, and pSS mice treated with Imq exhibited a significant loss of salivary flow that was more pronounced than that observed in the sham treatment group. Pulmonary and renal inflammation were enhanced in NOD.B10 mice that received Imq, and total IgG was elevated in the sera of these animals compared to BL/10 females that also received Imq treatment. Autoantibodies were also enriched in pSS mice following TLR7 agonism. Finally, the percentage of activated/memory cLN $CD4^+$ T cells were increased and T-bet^+ B cells (also referred to as age-associated B cells or ABCs) were

10.3389/fimmu.2022.1034336

dramatically expanded in Imq-treated pSS animals. Thus, TLR7 agonism drives local and systemic pSS disease, and resulted in accelerated disease in the context of pSS.

2 Materials and methods

2.1 Mice

C57BL/10 (BL/10) (stock #000666) and NOD.B10Sn-*H2*^{b} (NOD.B10) (stock #002591) were obtained from Jackson Labs. Animals were bred and maintained at the University of Buffalo laboratory animal facility in accordance with IACUC and NIH guidelines. All animals used in this study were female.

2.2 Treatment regimen

NOD.B10 female mice at a pre-disease stage (6 weeks of age) were given a sham base cream or 5% Imq cream. The Imq-containing cream was identical to the sham, with the exception of the addition of Imq. The treatments were administered epicutaneously to the ear three times a week for 6 weeks, as previously described (40). Parallel studies were performed using age and sex-matched healthy BL/10 controls. A detailed description of the treatment groups is provided in Supplementary Table 1.

2.3 Saliva and sera collection

Saliva was collected as previously described (7). Briefly, mice were injected with 0.3 mg/mL pilocarpine HCL (Sigma Aldrich) and saliva was collected for ten minutes on ice. Saliva was centrifuged and the volume assessed using a pipette. Saliva was collected prior to any treatment (5 weeks of age) and before euthanasia (12 weeks of age). Sera were harvested upon euthanasia by cardiac puncture. Blood was incubated at room temperature for 2 hours, and centrifuged at 0.7 g for 20 minutes. Sera were collected and frozen at -20 °C until use.

2.4 ELISAs

ELISAs were performed to quantify levels of IgM and IgG (Bethyl Laboratories), BAFF (R&D Systems), and β2-microglobulin (Lifespan Biosciences). Serial dilutions were prepared and values were calculated in accordance with manufacturer instructions. All samples were evaluated in duplicate.

2.5 HEp2 staining and autoantigen arrays

HEp2 staining was performed as previously described (7). Briefly, sera were diluted and incubated with HEp2 slides (Bion Enterprises) and goat anti-mouse IgG-Alexa 488 (Southern Biotech, 1.1 μg/mL) was used to detect the presence of anti-nuclear autoantibodies (ANAs). Slides were imaged using an Andor Dragonfly Microscope with a 20X glycerol objective (NA 0.75). Indirect immunofluorescence staining patterns were classified according to the ICAP using ImageJ after normalizing to the median intensity of each group (41). Autoantigen arrays were performed in collaboration with the UT Southwestern Genomics and Microarray Core Facility as previously described (7).

2.6 Flow cytometry

Spleens and cLNs were harvested and dissociated by mechanical dispersion. Following RBC lysis with ACK Lysis Buffer (Lonza), cells were incubated with Fc block (CD16/32, clone 2.4G2, BD Biosciences) and treated with antibodies directed against the following as indicated: B220 (clone RA3-6B2, BD Biosciences), CD23 (clone B3B4, Biolegend), CD21/35 (clone 7G6, BD Biosciences), T-bet (clone 4B10, BD Biosciences), CD11c (clone HL3, BD Biosciences), CD4 (clone GK1.5, BD Biosciences), CD8α (clone 53-6.7, BD Biosciences), CD44 (clone IM7, BD Biosciences), CD62L (clone MEL-14, BD Biosciences), CD138 (clone 281-2, BD Biosciences), CD69 (clone H1.2F3, Biolegend), and TLR7 (clone A94B10, BD Biosciences). Data were acquired using a BD Biosciences Fortessa and analyzed with FlowJo software (BD Biosciences).

2.7 Tissue collection and histological assessment

Submandibular salivary glands (SMGs), parotid salivary glands, lacrimal glands, lung and kidneys were harvested, tissue was fixed in 10% formalin and paraffin-embedded. Tissues were sectioned and stained with H&E. Slides were scanned using an Aperio ScanScope system (Leica Biosystems) with a 20X objective and 0.75 numerical aperture. Image/Fiji (version 1.53c) was used to measure the lymphocytic infiltration present in the tissues (42–44). The percent of lymphocytic infiltration was quantified by dividing the area of tissue occupied by lymphocytes by the total area of tissue examined and multiplying the value by 100.

2.8 Statistics

Autoantigen array data were analyzed using previously described methods (7). Briefly, for each comparison of two groups (BL/10 sham-treated versus BL/10 Imq-treated, NOD.B10 sham-treated versus NOD.B10 Imq-treated, BL/10 Imq-treated versus NOD.B10 Imq-treated, and BL/10 sham-treated versus NOD.B10 sham-treated) we first performed the two-sample t-test for all autoantigens, and then used the *p. adjust* R function in the stats R package to adjust the p-values in order to control the false discovery rate (45). The method proposed by Benjamini and Yekutieli was used in the adjustments (46). An autoantigen was deemed significant if the corresponding adjusted p-value was less than 0.05. The autoantigen array data is deposited in the Gene Expression Omnibus (GEO) database under the accession number GSE212467. Where appropriate, all other data were analyzed using paired student-T tests or ANOVA (Kruskal-Wallis test with multiple comparisons). All analyses were performed using the R programming language and Prism software (GraphPad) (47).

3 Results

3.1 Imq-treated pSS mice developed splenomegaly, cervical lymphadenopathy and expansion of TLR7-expressing B cells

To determine if TLR7 agonism accelerates pSS pathogenesis, we administered the TLR7 agonist Imq or sham base cream to pre-disease NOD.B10 females. Parallel experiments were performed in age and sex-matched BL/10 mice. An overview of the treatment timeline is provided in Figure 1A. BL/10 mice were treated in 3 individual groups, and NOD.B10 mice were treated in 4 groups. Data from each strain and treatment group were pooled from multiple experiments. An overview of the treatment groups is provided in Supplementary Table 1. Imq-treated BL/10 and NOD.B10 strains exhibited splenomegaly and cervical lymphadenopathy compared to sham-treated controls, and NOD.B10 mice had significantly higher spleen weights than sham-treated counterparts ($p = 0.0001$). BL/10 mice, in contrast, showed no difference in spleen weights between sham and Imq-treated groups (Figure 1B).

Since B cells are integral to pSS pathogenesis and TLR7 is highly expressed in the B cell compartment, we sought to determine if B cell TLR7 expression was altered following Imq treatment. There were no significant differences in the percentage of splenic B cells expressing TLR7 between the sham or Imq-treated strains in BL/10 or NOD.B10 mice. The percentage of B cells expressing TLR7 was upregulated in Imq-treated NOD.B10 mice, however, as compared to B cells derived from Imq-treated BL/10 controls ($p = 0.01$) (Figure 1C). The percentage of $TLR7^+$ cLN B cells was similar between sham and Imq-treated BL/10 mice, although Imq treatment caused an increase in this population in pSS mice as compared to sham-treated NOD.B10 controls ($p = 0.03$). Additionally, the cLN B cell population derived from Imq-treated NOD.B10 mice that expressed TLR7 was expanded compared to B cells derived from Imq-treated BL/10 mice ($p = 0.009$) (Figure 1C). Finally, the percentage of activated splenic and cLN B cells expressing TLR7 did not differ between sham and Imq-treated groups in both BL/10 or NOD.B10 mice (Figure 1D), although the percentage of activated $TLR7^+$ splenic B cells derived from sham-treated NOD.B10 mice was elevated as compared to those derived from sham-treated BL/10 females ($p = 0.02$). In addition, the percentage of activated $TLR7^+$ splenic B cells was elevated in Imq-treated pSS mice and compared to their BL/10 counterparts ($p = 0.01$) (Figure 1D). Finally, activated $TLR7^+$ splenic and cLN B cells derived from Imq-treated NOD.B10 animals were expanded as compared to those derived from Imq-treated BL/10 mice ($p = 0.0005$) (Figure 1D). Thus, TLR7 agonism induces cervical lymphadenopathy, splenomegaly, and expansion of TLR7-expressing B cells in secondary lymphoid organs, and these changes are more pronounced in pSS mice as compared to healthy controls.

3.2 TLR7 agonism induces sialadenitis, dacryoadenitis and loss of salivary flow

We next evaluated exocrine gland inflammation and loss of salivary flow in each of the treatment groups, as these are hallmarks of pSS. Sialadenitis in the submandibular gland was increased in BL/10 and NOD.B10 mice that received Imq treatment as compared to sham-treated controls, ($p = 0.01$ and $p = 0.003$ respectively). Of note, the parotid glands were spared from inflammation in all treatment groups, as lymphocytic infiltration was only observed in 1 NOD.B10 Imq-treated mouse (Supplementary Figure 1). Dacryoadenitis was enhanced in BL/10 and NOD.B10 mice that received Imq treatment as compared to sham-treated controls ($p = 0.02$ and $p = 0.001$, respectively), although there were no differences observed in either salivary or lacrimal inflammation between BL/10 and NOD.B10 mice that received Imq (Figures 2A, B).

To examine whether salivary gland function was altered following TLR7 activation, we quantified salivary production in all groups at pre- and post-treatment time points (Figure 1A). Salivary flow remained unchanged in BL/10 animals that received either sham cream or Imq (Figure 2C). In pSS mice, both sham and Imq-treated animals lost salivary flow over time ($p = 0.01$ and $p < 0.0001$, respectively). These changes, however, were more pronounced in animals that received Imq as compared to the sham treatment group (Figure 2C). Therefore, TLR7-mediated signals mediated exocrine inflammation and salivary hypofunction.

10.3389/fimmu.2022.1034336

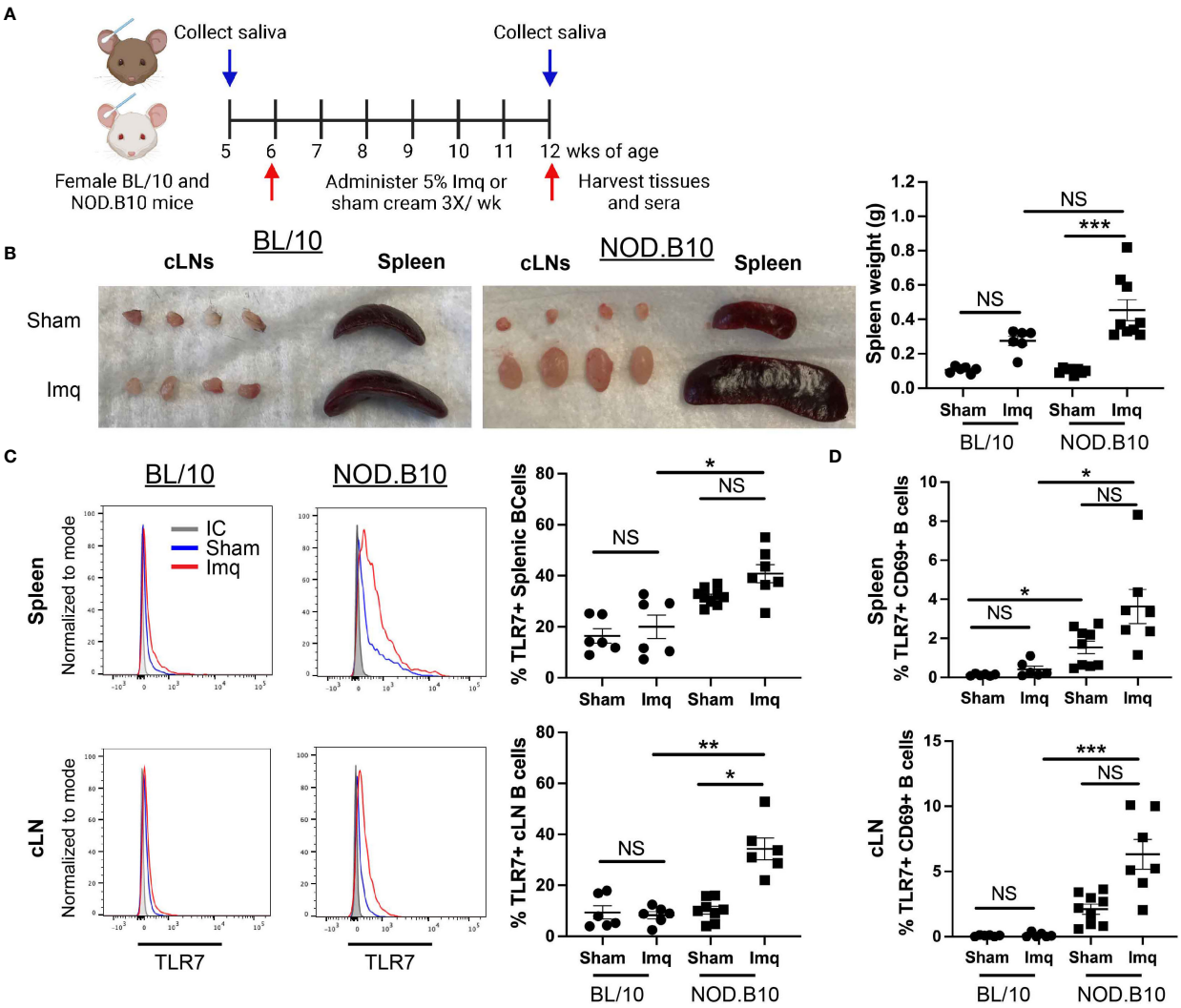

FIGURE 1
TLR7 agonism induces splenomegaly, cervical lymphadenopathy and expansion of TLR7-expressing B cells in NOD.B10 mice. **(A)** NOD.B10 and BL/10 mice were treated with sham or Imq-containing cream beginning at 6 weeks of age for 6 weeks. The treatment timeline is shown. **(B)** Representative images of spleen and cLNs from each treatment group and quantification of spleen weights is shown (n = 6 BL/10 sham, 6 BL/10 Imq-treated, 8 NOD.B10 sham, and 9 NOD.B10 Imq-treated mice). **(C)** Spleens and cLNs of sham (n = 6 BL/10 and 9 NOD.B10) or Imq-treated mice (n = 6 BL/10 and 7 NOD.B10) were harvested and flow cytometry was performed. Cells were gated on B220 and expression of TLR7 is shown. The percentages of $B220^+$, $TLR7^+$ B cells are quantified for spleen and cLNs, respectively. **(D)** Cells were gated on B220, and the percentages of cells in spleen and cLNs expressing TLR7 and CD69 are shown. Horizontal lines represent the mean and SEM (NS, non-significant, *p < 0.05, ***p < 0.001, and ***p < 0.0001).

3.3 TLR7 agonism induced pulmonary and renal inflammation in pre-disease NOD.B10 mice

To determine if TLR7 stimulation induces systemic inflammation in pSS mice that is characteristic of pSS patients, we assessed pulmonary and renal inflammation in each of the treatment groups. There were no significant differences in the area of lymphocytic infiltration in either lung or kidney tissue in BL/10 mice treated with Imq as compared to strain-matched sham controls (Figures 3A, B). In contrast, TLR7 activation induced interstitial pneumonitis and nephritis in pSS mice (p = 0.04 and 0.02, respectively), although there was no difference in inflammation in either tissue between Imq-treated BL/10 and NOD.B10 mice (Figures 3A, B). All of the Imq-treated NOD.B10 mice displayed perivascular lymphoplasmacytic inflammation in the kidney, concentrated at the pelvis but tracking into the medulla and cortex in some cases (Figure 3B). In addition, kidneys from 3 of the NOD.B10 Imq-treated mice had evidence of glomerular damage (proteinuria), which was scored as

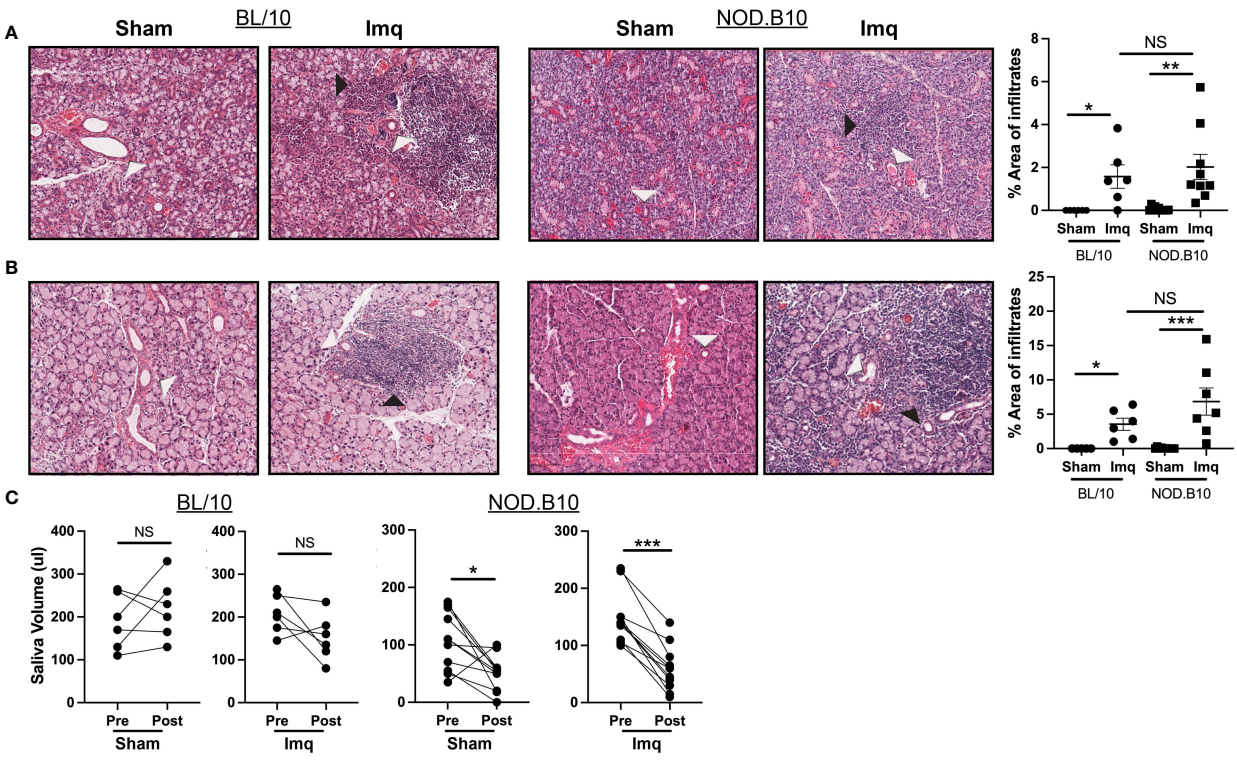

FIGURE 2
pSS mice treated with Imq exhibit robust lymphocytic infiltration of exocrine tissues and loss of salivary flow. **(A)** SMG and **(B)** lacrimal tissues were harvested from sham (n = 10) or Imq-treated female mice (n = 9) and from sham (n = 6) or Imq-treated age and sex-matched controls (n = 6). One representative photomicrograph is shown from each group. White arrows indicate exocrine gland ducts and black arrows indicate inflammation. Lymphocytic infiltration was quantified using ImageJ. Horizontal lines represent the mean and SEM **(C)** Stimulated saliva was collected prior to treatment and at the conclusion of the experiment from BL/10 and NOD.B10 mice. (NS = non-significant, *p < 0.05, **p < 0.001, ***p < 0.001).

minimal (n = 1/9), mild (n = 1/9), or severe (n = 1/9). None of the Imq-treated BL/10 mice exhibited glomerular damage. Therefore, TLR7 agonism drives systemic inflammation that is characteristic of pSS.

3.4 Total and ANA-specific antibodies are increased in pSS mice following TLR7 activation

We next assessed total and ANA-specific antibodies in sham and Imq-treated BL/10 and NOD.B10 mice. There were no differences in total IgM or IgG titers between sham and Imq-treated strains in both BL/10 and NOD.B10 mice. We noted a significant increase, however, in total IgG titers when comparing Imq-treated NOD.B10 mice to their BL/10 counterparts (p = 0.0003) (Figure 4A). We next performed HEp2 assays to evaluate ANA-specific IgG antibodies in the sera of pSS mice. Of note, we did not carry out these analyses in the BL/10 treatment groups, as IgG titers were low and remained unchanged following Imq treatment. We observed negligible ANAs in most of the sham-treated pSS mice (7/11), although a minority of animals displayed nucleolar homogenous (1/11) or nuclear speckled patterns (3/11) (Figure 4B). We then analyzed the Imq-treated pSS mice. In contrast, all animals displayed ANA-specific IgG autoantibodies. The majority of the sera examined displayed a nuclear speckled pattern (6/7), while a cytoplasmic speckled pattern was observed in one of mice examined (1/7) (Figure 4B). Thus, TLR7 agonism induced ANA production in Imq-treated pSS mice, and the patterns observed were consistent with RNA-associated autoantigens.

3.5 RNA-associated autoantigens are increased in pSS mice following Imq treatment

To confirm and extend the ELISA and HEp2 studies, we performed autoantigen arrays on sera derived from sham or Imq-treated BL/10 and NOD.B10 mice. We focused our analyses on ANA-specific IgM and IgG (Figure 5). We first examined whether ANAs were elevated in sera from BL/10 mice treated

10.3389/fimmu.2022.1034336

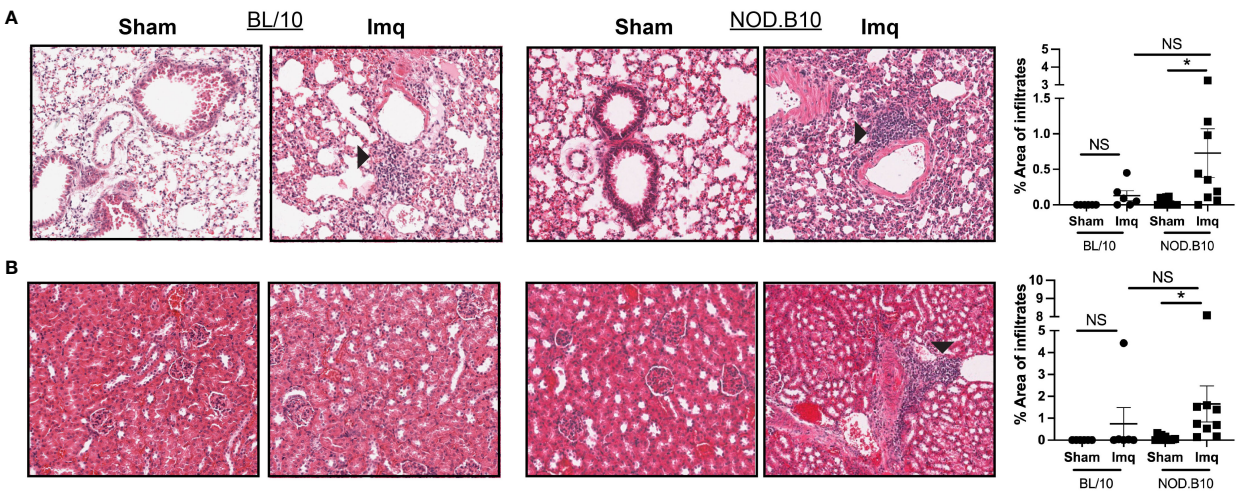

FIGURE 3
TLR7 agonism induces significant pulmonary and renal inflammation in pSS mice. **(A)** Lung and **(B)** kidney tissues were harvested from sham (n = 10) or Imq-treated female pSS mice (n = 9) and from sham (n = 6) or Imq-treated age and sex-matched controls (n = 6). One representative photomicrograph is shown from each group. Lymphocytic infiltration was quantified using ImageJ and black arrows indicate tissue inflammation. Horizontal lines represent the mean and SEM (NS = non-significant, *p < 0.05).

with Imq as compared to sham controls. We found IgM autoantibodies directed against SmD (p = 0.001), ssDNA (p = 0.04), SP100 (p = 0.02), gp210 (p = 0.006), genomic DNA (p = 0.003), and U1-snRNP 68/70 kDa (p = 0.002) were elevated in Imq-treated mice (Figures 5A, B). Additionally, IgG autoantibodies directed against genomic DNA (p = 0.01), PL-7 (p = 0.006), U1-snRNP-A (p = 0.005), Jo-1 (p = 0.002), Ku (p70/p80) (p = 0.001), Nup62 (p = 0.001), PL-12 (p = 0.001), and U1-snRNP 68/70 kDa (p = 0.001) were elevated in Imq-treated BL/10 mice (Figures 5C, D). We next examined autoantibodies in sham and Imq-treated NOD.B10 mice. As expected, we found enrichment of numerous IgM and IgG specific ANAs in the sera from NOD.B10 mice, and many of them recognized ribonuclear proteins. Indeed, IgM directed against U1-snRNP-A (p = 0.05), PL-7 (p = 0.04), nucleosome (p = 0.03), histone (p = 0.02), Ku (p70/p80) (p = 0.02), SRP54 (p = 0.02), genomic DNA (p = 0.02), La/SSB (p = 0.02), PL-12 (p = 0.02), ssDNA (p = 0.01), TIF1-γ (p = 0.01), Sm (p = 0.01), PM/Scl-100 (p = 0.008), Scl-70 (p = 0.007), SP100 (p = 0.006), nucleolin (p = 0.006), SmD1 (p = 0.006), Nup62 (p = 0.005), dsDNA (p = 0.005), Mi-2 (p = 0.005), Sm/RNP (p = 0.005), CENP-A (p = 0.003), CENP-B (p = 0.003), PM/Scl-75 (p = 0.003), Ro/SSA (60 kDa) (p = 0.003), DFS70 (p = 0.003), U1-snRNP 68/70 kDa (p = 0.001), Ro/SSA (52 kDa), U1-snRNP-C (p = 0.001), SmD (p = 0.001), and U1-snRNP-B/B were enriched in Imq-treated mice as compared to sham controls (Figures 5A, B). Finally, ANA-specific IgG was also elevated in the NOD.B10-treated mice, as TIF1-γ (p = 0.03), SmD1 (p = 0.03), gp210 (p = 0.03), U-snRNP-B/B (p = 0.02), PM/Scl-100 (p = 0.01), Scl-70 (p = 0.01), Ku (p70/p80) (p = 0.009), Mi-2 (p = 0.009), dsDNA (p = 0.008), nucleolin (p = 0.006), Nup62 (p = 0.006), PM/Scl-75, (p = 0.006), Ro/SSA (52 kDa) (p = 0.006), Histone (p = 0.005), PL-12 (p = 0.005), Ro/SSA (60 kDa) (p = 0.004), La/SSB (p = 0.002), U1-snRNP-C (p = 0.002), and U1-snRNP 68/70 kDa (p = 0.001) were elevated. Of note, there were no differences observed between Imq-treated BL/10 and NOD.B10 animals in either IgM or IgG autoreactivity, although both ANA-specific IgM and IgG were elevated in NOD.B10 sham-treated animals as compared to analogous BL/10 mice (Supplementary Figure 2).

3.6 TLR7 agonism resulted in the expansion of activated/memory T cells and T-bet$^+$ B cells

Since autoantibodies were elevated in pSS mice following Imq treatment, we performed studies to evaluate CD4$^+$ and CD8$^+$ T cell populations and T-bet$^+$ B cells in the spleens and cLNs of each treatment group. There were no differences in the percentage of CD4$^+$ T cells in either the spleens or cLNs from derived from BL/10 or NOD.B10 mice in any of the groups (Supplementary Figures 3A, C). In addition, the percentage of splenic CD8+ T cells was unchanged between BL/10 sham and Imq-treated animals, although this population was significantly diminished in the Imq-treated NOD.B10 mice as compared to sham-treated controls (p = 0.0004) (Supplementary Figure 3B). In the cLNs, the percentage of CD8$^+$ T cells was decreased significantly in both Imq-treated NOD.B10 and BL/10 mice as compared to sham-treated controls of the same strain (p = 0.04 and p = 0.01, respectively) (Supplementary Figure 3D).

10.3389/fimmu.2022.1034336

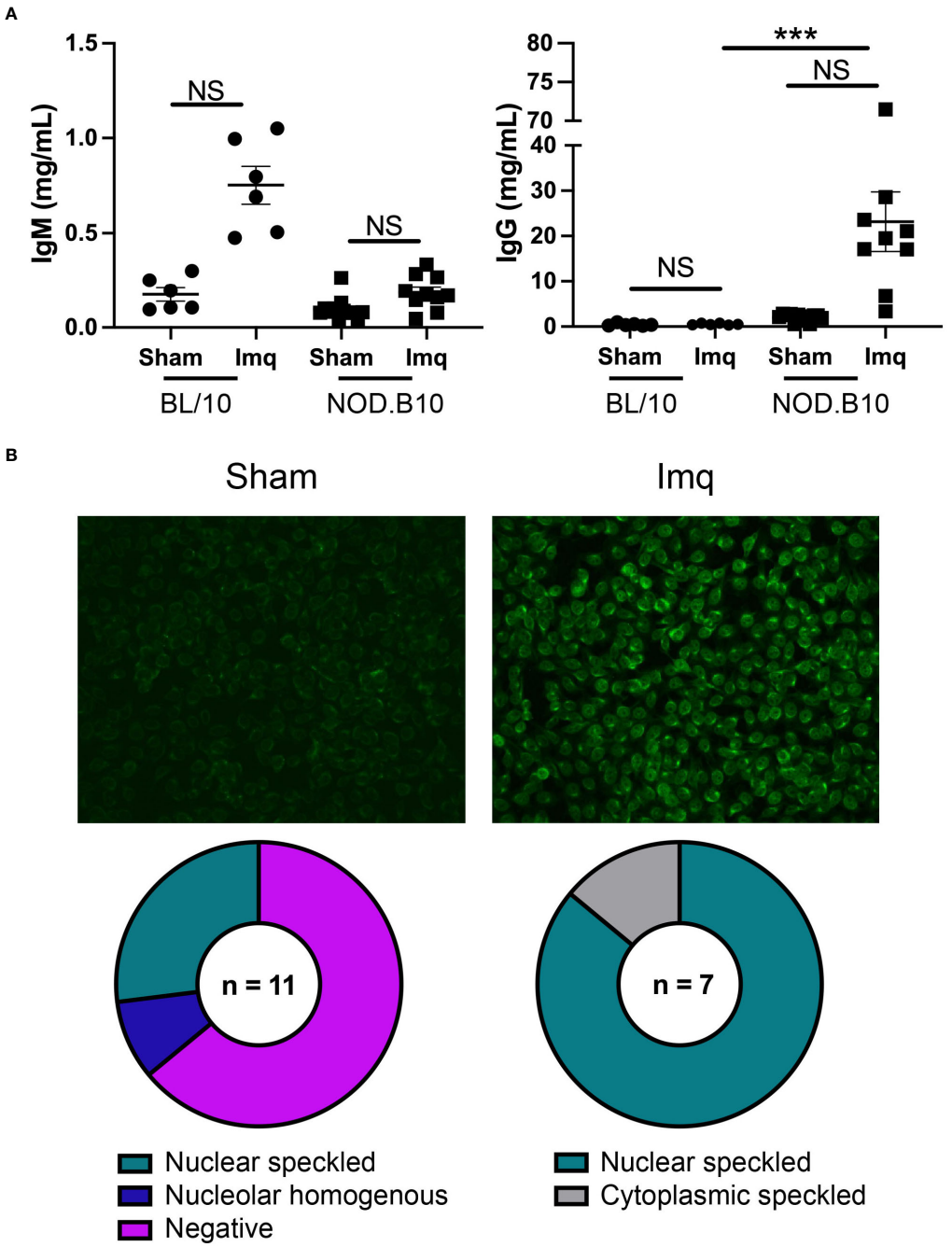

FIGURE 4
NOD.B10 mice treated with Imq demonstrate high IgG titers and ANA levels. Sera were harvested from NOD.B10 sham (n = 10) and Imq-treated female mice (n = 9) and from BL/10 sham (n = 6) and Imq-treated female BL/10 mice (n = 6) by cardiac puncture following euthanasia. **(A)** Total IgM and IgG titers were quantified by ELISA. Horizontal lines represent the mean and SEM (NS, non-significant, ****p < 0.0001). **(B)** Anti-nuclear autoantibodies were detected by HEp2 staining. One representative image is shown from each group.

We next assessed $CD4^+$ and $CD8^+$ activated/memory B cells in spleens and cLNs. We found that the percentage of splenic activated/memory $CD4^+$ T cells was increased significantly in Imq-treated BL/10 mice compared to the sham controls ($p = 0.003$), although there was no difference in this population in spleens derived from sham and Imq-treated NOD.B10 mice. Moreover, the percentage of splenic activated/memory $CD4^+$ T cells was similar in Imq-treated BL/10 and

10.3389/fimmu.2022.1034336

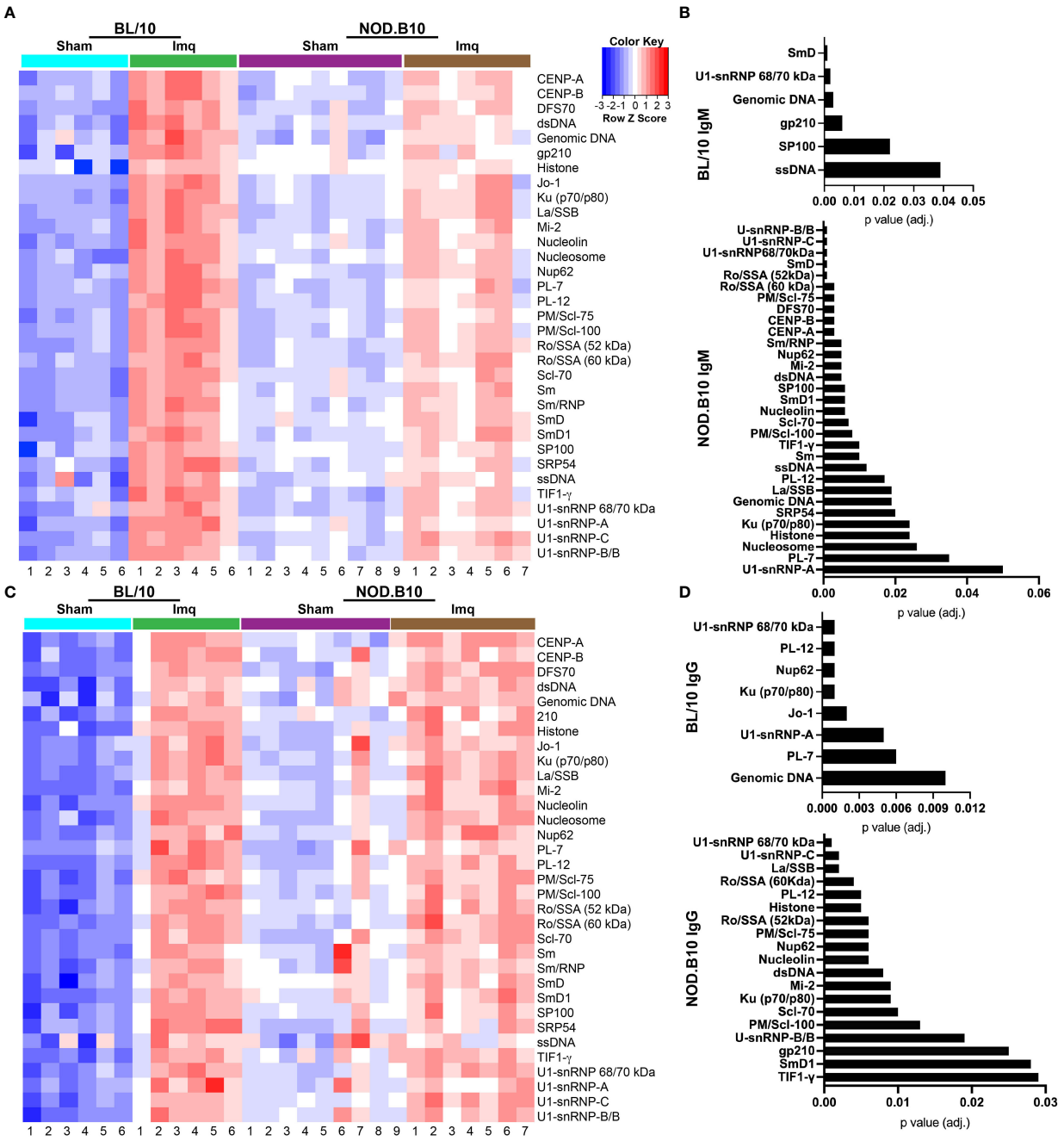

FIGURE 5
Autoantigen arrays reveal enrichment of autoantibodies in the sera of Imq-treated NOD.B10 mice. Sera were harvested from NOD.B10 sham (n = 9) or Imq-treated female mice (n = 7) by cardiac puncture following euthanasia. Sera were harvested similarly from BL/10 sham (n = 6) or Imq-treated female BL/10 mice (n = 6). Autoantigen arrays were performed and heatmaps for ANA-specific **(A)** IgM and **(C)** IgG are shown. ANA-specific **(B)** IgM and **(D)** IgG that was significantly enriched in Imq-treated BL/10 and NOD.B10 mice as compared to sham-treated strain-matched controls is shown.

NOD.B10 animals (Figure 6A). In contrast, cLN activated/memory $CD4^+$ T cells were expanded in both BL/10 and NOD.B10 Imq-treated mice as compared to their sham-treated counterparts ($p = 0.02$ and $p = 0.01$, respectively) (Figure 6A). Of note, there was no significant difference the activated/memory $CD4^+$ T cell populations in Imq-treated cLNs derived from NOD.B10 mice as compared to those derived from Imq-treated BL/10 animals (Figure 6A).

10.3389/fimmu.2022.1034336

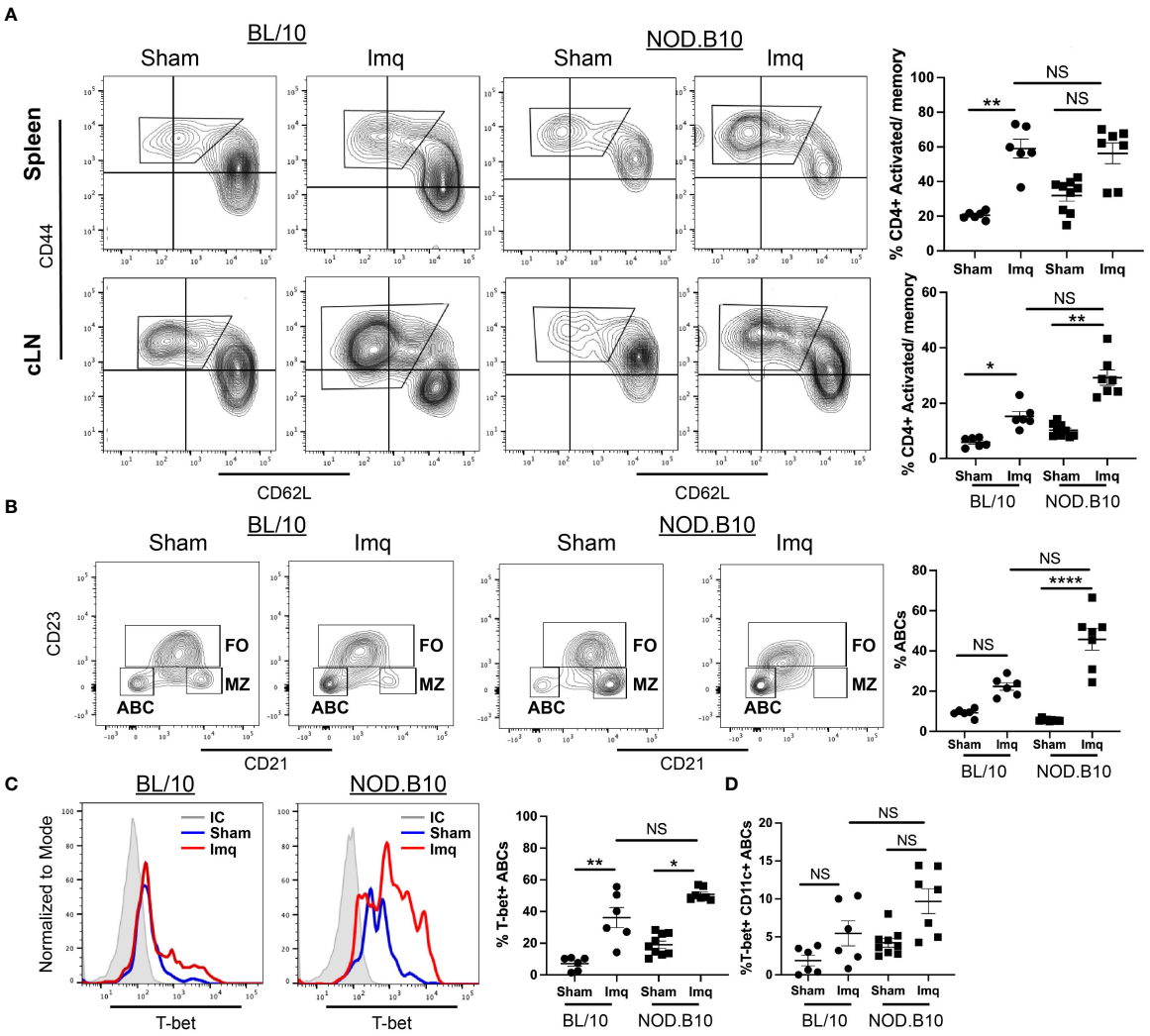

FIGURE 6
Activated/memory T cells and T-bet-expressing B cells are expanded in secondary lymphoid organs of pSS mice. Spleens and cLNs of sham (n = 9) or Imq-treated NOD.B10 mice (n = 7) and from sham (n = 6) or Imq-treated age and sex-matched controls (n = 6) were harvested and flow cytometry was performed. **(A)** Cells were gated on CD4 and CD44 and CD62L expression is shown. The percentages of activated/memory T cells ($CD4^+$, $CD44^+$, $CD62L^-$) from spleen and cLNs are shown. **(B)** The percentages of ABCs ($B220^+$, $CD21^-$, $CD23^-$) were quantified. ABCs were gated and expression of **(C)** T-bet and **(D)** Tbet/CD11c are shown. Plots from one representative animal from each group is shown. Horizontal lines represent mean and SEM (NS, non-significant, *p < 0.05, **p < 0.01, ****p < 0.0001).

$CD8^+$ activated/memory T cells were expanded in the spleen of BL/10 mice following Imq treatment (p = 0.0006), and no changes were observed in this population in Imq-treated NOD.B10 mice as compared to sham-treated controls (Supplementary Figure 3E). Finally, the percentage of activated/memory $CD8^+$ T cells remained unchanged in cLNs from both BL/10 and NOD.B10 Imq-treated mice as compared to sham controls (Supplementary Figure 3F). In contrast, in NOD.B10 sham-treated mice showed a higher percentage of activated/memory CD8+ T cells as compared to sham-treated BL/10 mice (p = 0.004) (Supplementary Figure 3F).

To assess if B cell populations were altered following TLR7 agonism, we assessed the percentage of total B cells, as well as the Fo and MZ B cell populations in our treatment groups. We found that the percentages of total splenic and cLN B cells and Fo B cells in the spleen did not differ between sham and Imq-treated strains in both BL/10 and NOD.B10 mice (Supplementary Figures 4A, B, D). Additionally, there was no change in the percentage of MZ B cells between sham and Imq-treated BL/10 mice. In contrast, Imq-treated MZ B cells from NOD.B10 mice were decreased dramatically as compared to those from NOD.B10 sham controls (p < 0.0001) (Supplementary Figure 4C). Additional

studies were performed to assess BAFF levels in the sera of sham and Imq-treated mice. We found that Imq-treated NOD.B10 mice had elevated serum BAFF levels as compared to their sham-treated counterparts ($p = 0.049$). While BAFF levels tended to be higher in the BL/10 Imq-treated mice as compared to sham-treated controls, this difference did not reach statistical significance ($p = 0.053$) (Supplementary Figure 4E). Finally, serum β2-microglobulin levels were assessed. We found that β2-microglobulin was elevated in the sera of Imq-treated NOD.B10 mice as compared to sham-treated NOD.B10 controls ($p = 0.02$). There was no difference between sham and Imq-treated BL/10 mice, or between Imq-treated BL/10 and NOD.B10 mice (Supplementary Figure 4F).

We next assessed the splenic ABC populations in sham and Imq-treated mice. The percentage of ABCs ($B220^+$, $CD21^-$, $CD23^-$) in sham and Imq-treated BL/10 animals was similar (Figure 6B). In contrast, we observed a significant expansion of ABCs derived from Imq-treated NOD.B10 mice as compared to sham controls ($p < 0.0001$) (Figure 6B). We then assessed the percentage of ABCs that expressed T-bet and CD11c, as these markers are characteristic of ABCs, and identify distinct subsets within this population. We found that T-bet expression was significantly higher in ABCs derived from Imq-treated strains than sham controls in both BL/10 and NOD.B10 animals ($p = 0.008$ and 0.02, respectively) (Figure 6C). However, there was no difference in T-bet expression in ABCs derived from Imq-treated NOD.B10 mice as compared to those from Imq-treated BL/10 mice (Figure 6C). Lastly, there were no significant differences in the percentage of ABCs that expressed T-bet and CD11c between Imq-treated strains and sham controls in both BL/10 and NOD.B10 animals (Figure 6D). Finally, we examined the percentage of splenic monocytic cells ($B220^-$, $CD11c^+$) in each of the treatment groups. We found no differences between the percentage of $CD11c^+$ cells in spleens derived from BL/10 mice when we compared sham and Imq-treated mice. In addition, the percentage of $CD11c^+$ cells was similar between Imq-treated BL/10 and NOD.B10 mice. When we examined the CD11c-expressing monocytes in NOD.B10 mice, however, we found that Imq-treated mice exhibited higher levels of this population as compared to sham-treated counterparts ($p = 0.007$) (Supplementary Figure 5). Thus, treatment of pSS mice with a TLR7 agonist results in the expansion of activated/memory $CD4^+$ T cells, T-bet^+ B cells, and $CD11c^+$ monocytes.

4 Discussion

4.1 TLR7 signaling mediates local and systemic pSS disease

Our study revealed that pre-disease stage pSS mice develop accelerated local and systemic pSS manifestations in response to treatment with the TLR7 agonist Imq. Salivary and lacrimal inflammation were increased as compared to sham-treated NOD.B10 controls in response to Imq treatment, although the area occupied by lymphocytes in exocrine tissue did not differ between Imq-treated BL/10 and NOD.B10 mice (Figures 2A and B). Salivary flow, however, was reduced in pSS mice treated with Imq, while saliva production remained unchanged in healthy controls following Imq administration (Figure 2C). In agreement with the literature, these data suggest that salivary hypofunction is not mediated exclusively by the presence of lymphocytic infiltrates within salivary tissue, and other factors, such as apoptosis and anti-muscarinic 3 receptor autoantibodies, likely contribute to the dryness observed (48–51). This finding also raises the intriguing possibility that TLR7 activation in the parenchymal compartment could be a prime driver of the salivary dysfunction observed in pSS mice, although further studies in TLR7-deficient models are needed to establish this conclusively.

In contrast to our findings in exocrine tissue, inflammation was increased in the lungs and kidneys from pSS mice in response to Imq treatment, and this was not observed in the analogous BL/10 treatment group (Figure 3). Whether this observation relates to intrinsic differences in the pulmonary and renal microenvironments in NOD.B10 mice, and/or whether this inflammation is driven primarily by TLR7-mediated peripheral immune cell activation remains to be determined.

The exocrine-specific and extraglandular disease manifestations were similar when we compared the Imq-treated NOD.B10 mice to NOD.B10 female mice at the clinical disease stage that develop pSS spontaneously. Differences, however, were observed in the antibody repertoire of Imq-treated mice as compared to pSS mice as the clinical disease stage. Indeed, HEp2 staining of NOD.B10 Imq-treated mice revealed that their sera displayed primarily a speckled pattern, while only a minority of the serum samples derived from NOD.B10 mice at 6 months of age exhibited a speckled pattern (4/15 animals) (7). In addition, IgM titers were not increased in Imq-treated animals, while these are elevated in NOD.B10 mice that developed disease spontaneously (7, 39). Finally, cervical lymphadenopathy and splenomegaly were observed in Imq-treated mice, while this is not characteristic of NOD.B10 females that develop the disease spontaneously (7). While we do not know the reason for these differences, we suspect that in spontaneous disease many other factors besides TLR7 activation contribute to disease development, as additional MyD88-dependent and -independent signaling cascades are implicated (6, 52–55). Thus, while TLR7 agonism recapitulates many features of pSS disease that develop spontaneously in this model, other inflammatory networks likely contribute to disease. Table 1 provides a comparison of the findings in Imq-treated NOD.B10 mice with those observed in NOD.B10 mice at the clinical disease stage.

10.3389/fimmu.2022.1034336

TABLE 1 Comparison of Disease Manifestations between Imq-treated NOD.B10 mice and clinical disease stage NOD.B10 females.

	Imq-induced	Clinical disease (spontaneous)
Sialadenitis - SMG	Yes	Yes
Sialadenitis- Parotid	Negligible	Negligible
Hyposalivation	Yes	Yes
Dacryoadenitis	Yes	Yes
Nephritis	Yes	Yes
Pneumonitis	Yes	Yes
Elevated serum IgM	No	Yes
Elevated serum IgG	Yes	Yes
Autoantibodies	Yes	Yes
Splenomegaly	Yes	No
Cervical Lymphadenopathy	Yes	Minimal

4.2 TLR7 signaling cascades are critical for the development and expansion of ABCs

Activation of distinct B cell subsets by TLR7 ligands is integral to autoimmunity, and elegant studies conducted over the past decade have revealed an important role for ABCs in mouse models of lupus pathogenesis (17, 56–59). Of direct relevance to the current study, TLR7 is required for ABC expansion in the context of lupus (57, 58), and B cells that express T-bet drive lupus-like disease in mice (56). Importantly, following stimulation with a TLR7 agonist, ABCs derived from healthy mice secrete heightened IgM and IgG (58). Additionally, ABCs from NZB/WF1 lupus mice produce high levels of IgG autoantibodies as compared to other B cell subsets derived from the same strain (58), and corroborative *in vivo* studies demonstrate that depletion of the ABC subset leads to a reduction in autoantibody titers (58). Subsequent work revealed that T-bet$^+$ B cells mediate autoantibody production in the context of lupus (56). Significantly, ablation of T-bet$^+$ B cells diminished germinal centers, protected against kidney damage, and reduced B and T cell activation (56), demonstrating that ABCs play an essential role in autoimmunity.

4.3 T-bet$^+$ B cells are expanded in pSS mice in response to TLR7 activation

We found high titers of total and autoreactive IgG in pSS mice following TLR7 agonism (Figures 4, 5). This was accompanied by dramatic expansion of splenic ABCs (B220$^+$, CD23$^-$, CD21$^-$, T-bet$^+$ B cells) that was greater than that observed in sham controls and BL/10 Imq-treated animals (Figures 4A, 6B, C). Moreover, stimulation of pre-disease pSS females with Imq resulted in elevated percentages of B cells expressing TLR7 in cLNs (Figure 1C). Furthermore, the percentage of activated B cells that expressed TLR7 was expanded in the spleens and cLNs of Imq-treated pSS mice as compared with the BL/10 treatment group that also received Imq (Figure 1D). Activated/memory CD4$^+$ T cells were also increased in the cLNs of Imq-treated mice (Figure 6A). It is interesting to speculate that this T cell expansion may be driven by the elevated percentages of T-bet$^+$ B cells observed in pSS mice following treatment.

Evidence for ABC-driven T cell expansion in autoimmunity is provided by data from a lupus model that exhibits excessive ABC accumulation (60). In this model, the ABC subset induced expansion and heightened proliferation of CD44$^+$CD62L$^-$ T effector memory cells as compared to the Fo B cell subset, and this was mediated by the potent antigen presentation function exhibited by ABCs (60). Altogether, this work suggests that TLR7 activation in the B cell compartment is integral to pSS disease progression, although further studies are needed to determine whether TLR7-induced T-bet$^+$ B cells are the prime driver of disease in our model, or whether organ-specific TLR7 activation of stromal and parenchymal cells also mediates pathology. Of note, these possibilities are not mutually exclusive, as TLR7 signals in diverse tissue microenvironments may activate distinct signaling networks that govern specific disease manifestations.

Our work is relevant to the human disease, as B cells that share both phenotypic and functional properties with murine ABCs are dysregulated in human autoimmunity (59). Of particular significance, CD19$^+$, CD21$^{-/lo}$ B cells are expanded in patients with pSS (61, 62). These cells are reminiscent of ABCs characterized in mice, as they are enriched in reactivity to nuclear and cytoplasmic autoantigens and they are responsive to TLR agonism (61, 62). In addition, CD21^{lo} B cells derived from patients with autoimmunity can serve as antigen presenting cells, as these cells express high levels of CD80, CD86 and HLA-DR (63–65). Recent work demonstrated that CD21^{lo} B cells consistently express high levels of T-bet and

differentiate in response to TLR agonism or T cell help (66). While the relevance of TLR signaling in the development and subsequent activation of the CD21^{lo} B cell subset requires further study, these data suggest that autoreactive CD21^{lo} B cells could be an important mediator of T cell activation in human autoimmunity, including pSS (66).

4.4 ABCs exhibit TLR7-driven sexual dimorphism in lupus and this likely contributes to the female disease predilection in pSS

It is important to note that pSS is primarily seen in middle-aged females, and the diagnosis in males is considerably more rare (1). Although the underlying molecular mechanisms that govern this striking sex predilection are not well-understood at present, emerging data suggest that improper X-chromosome inactivation (XCI) and subsequent gene dosage affects may account for the high disease prevalence observed in women (67). Accordingly, TLR7 is expressed on the X-chromosome and XCI escape in lymphocytes from SLE patients is well documented, resulting in elevated TLR7 expression (67). Recent work in mice that develop a lupus-like disease found that ABCs were preferentially expanded in females (68). In addition, female-derived ABCs from this model showed an enhanced IFN-gene signature as compared to ABCs derived from male counterparts. Intriguingly, overexpression of TLR7 in males reversed the sex-bias observed and resulted in heightened ABC-mediated pathology, culminating in lung pathology and diminished overall survival (68). While no studies to date have examined whether TLR7 expression and function are altered between males and females in the context of pSS, additional work is needed to determine whether ABCs are preferentially expanded in females and whether this may be in response to TLR-medicated signaling, as this may represent a previously unappreciated disease mechanism that underlies the high prevalence of disease observed in women.

4.5 Ro and La may serve as endogenous TLR7 ligands in pSS

Currently, the etiology of pSS is poorly understood and early disease events are not clearly defined. Therefore, it is of critical importance to understand how TLR7 becomes activated in the context of pSS. MRL/lpr lupus mice that lack TLR7 exhibit disease amelioration and diminished antibodies against RNA-associated antigens (69). Corroborative studies in a lupus mouse model revealed that increasing TLR7 gene dosage augments production of autoantibodies directed against RNA (70). These findings are relevant to human disease, as most patients with pSS and SLE display autoantibodies to Ro (SSA) and La (SSB) (71, 72). Both Ro and La are ribonuclear proteins that form complexes with RNA (73). It is hypothesized that the RNA in these complexes serves as an endogenous adjuvant to activate TLR7-expressing B cells and drive plasma cell differentiation. This may explain, at least in part, the extremely high titers of these autoantibodies observed in SLE patients (74, 75). It is interesting to note that NOD.B10 mice treated with Imq demonstrated enrichment of IgG autoantibodies directed against RNA-associated antibodies, such as Ro, La, U1-snRNP 68/70 kDa, U1-snRNP-C, U-snRNP-B/B, and SmD1 (Figure 5). Thus, it is possible that TLR7 activation of B cells may occur through Ro and La-mediated activation of B cells in the context of human disease, although further studies are needed to identify clinically-relevant sources of TLR7 activation in pSS patients.

5 Conclusion

In conclusion, TLR7 agonism accelerates both local and systemic disease manifestations in a mouse model of pSS. This work has important therapeutic relevance, as targeting of TLR7-dependent signaling networks may be efficacious in reducing B cell activation and tissue-specific inflammation that is characteristic of disease.

Data availability statement

The datasets presented in this study can be found in online repositories. The names of the repository/repositories and accession number(s) can be found on: https://www.ncbi.nlm.nih.gov/geo/, GSE212467.

Ethics statement

The animal study was reviewed and approved by University of Buffalo Institutional Animal Care and Use Committee.

Author contributions

JiK conceived of the work, wrote the manuscript and performed experiments. AP, EK, JeK, and JiK critically edited the manuscript and performed experiments. CZ performed the autoantigen arrays and normalized the data. JM critically edited the manuscript and analyzed the autoantigen arrays. All authors contributed to the article and approved the submitted version.

Funding

Funding for this work was provided by NIH/National Institute of Dental and Craniofacial Research (NIDCR) award R01DE29472 to JiK and AP received support from NIDCR award T32023526. Research reported in this publication was supported by the National Center for Advancing Translational

Sciences of the National Institutes of Health under award number UL1TR001412 to the University at Buffalo. The content is solely the responsibility of the authors and does not necessarily represent the official views of the NIH.

Acknowledgments

The authors thank Dr. Teresa Southard (Associate Professor of Anatomic Pathology, Virginia-Maryland Regional College of Veterinary Medicine) for her evaluation of histopathology in renal tissue. Instrumentation for this work was provided by the Optical Imaging and Analysis Facility at the University of Buffalo. Funding for this work was provided by NIH/National Institute of Dental and Craniofacial Research (NIDCR) award R01DE29472 to JiK and AP received support from NIDCR award T32023526. Research reported in this publication was supported by the National Center for Advancing Translational Sciences of the National Institutes of Health under award number UL1TR001412 to the University at Buffalo. The content is solely the responsibility of the authors and does not necessarily represent the official views of the NIH.

Conflict of interest

The authors declare that the research was conducted in the absence of any commercial or financial relationships that could be construed as a potential conflict of interest.

Publisher's note

Supplementary material

The Supplementary Material for this article can be found online at: https://www.frontiersin.org/articles/10.3389/fimmu.2022.1034336/full#supplementary-material

SUPPLEMENTARY FIGURE 1
Parotid gland tissue from both BL/10 and NOD.B10 mice exhibits negligible inflammation following Imq administration. Parotid tissues were harvested from sham (n = 10) or Imq-treated female mice (n = 9) and from sham (n = 6) or Imq-treated age and sex-matched controls (n = 6). One representative photomicrograph is shown from each group. Lymphocytic infiltration was quantified using ImageJ. White arrows represent salivary gland ducts. Horizontal lines represent the mean and SEM (NS = non-significant).

SUPPLEMENTARY FIGURE 2
Autoantigen arrays reveal enrichment of specific autoantibodies in sham-treated NOD.B10 mice as compared to BL/10 sham-treated controls. Sera were harvested from NOD.B10 (n = 9) or BL/10 sham controls (n = 6) by cardiac puncture following euthanasia. Autoantigen arrays were performed for **(A)** IgM and **(B)** IgG. Autoantibodies that were enriched in NOD.B10 animals are shown.

SUPPLEMENTARY FIGURE 3
The percentage of $CD8^+$ T cells are decreased in spleens and cLNs of Imq-treated mice. Spleens and cLNs of sham (n = 9) or Imq-treated NOD.B10 mice (n = 7) and from sham (n = 6) or Imq-treated age and sex-matched controls (n = 6) were harvested and flow cytometry was performed. The percentage of splenic and cLN **(A and C)** $CD4^+$ and **(B and D)** $CD8^+$ cells are shown. The percentages of activated/memory T cells ($CD8^+$, $CD44^+$, $CD62L^-$) from **(E)** spleen and **(F)** cLNs are shown. (NS, non-significant, *p < 0.05, **p < 0.01, ***p < 0.001).

SUPPLEMENTARY FIGURE 4
Marginal zone B cells are diminished in NOD.B10 mice following TLR7 agonism. Spleens and cLNs of sham (n = 9) or Imq-treated NOD.B10 mice (n = 7) and from sham (n = 6) or Imq-treated age and sex-matched controls (n = 6) were harvested and flow cytometry was performed. The percentage of **(A)** total splenic B cells ($B220^+$), **(B)** follicular B cells ($B220^+$, $CD23^+$, $CD21^{lo/-}$) and **(C)** marginal zone B cells ($B220^+$, $CD23^-$, $CD21^+$) are shown. **(D)** The percentage of B cells in the cLNs of BL/10 and NOD.B10 sham and imq-treated mice are shown. Sera were harvested and **(E)** BAFF levels were assessed in C57BL/10 sham and Imq-treated (n = 6 each) and NOD.B10 sham and Imq-treated animals (n = 10 each) following euthanasia. **(F)** Serum β2-microglobulin levels were assessed in C57BL/10 sham and Imq-treated (n = 6 each) and NOD.B10 sham and Imq-treated mice (n = 9 each) following euthanasia (NS, non-significant, *p < 0.05, ***p < 0.001).

SUPPLEMENTARY FIGURE 5
The percentages of $CD11c^+$ monocytes ($B220^-$, $CD11c^+$) were quantified. Histogram plots from one representative animal from each group are shown. Horizontal lines represent mean and SEM (NS, non-significant, **p < 0.01).

References

1. Mariette X, Criswell LA. Primary sjogren's syndrome. *N Engl J Med* (2018) 379(1):97. doi: 10.1056/NEJMcp1702514

2. Shiboski CH, Baer AN, Shiboski SC, Lam M, Challacombe S, Lanfranchi HE, et al. Natural history and predictors of progression to sjogren's syndrome among participants of the sjogren's international collaborative clinical alliance registry. *Arthritis Care Res (Hoboken)* (2018) 70(2):284–94. doi: 10.1002/acr.23264

3. Malladi AS, Sack KE, Shiboski SC, Shiboski CH, Baer AN, Banushree R, et al. Primary sjogren's syndrome as a systemic disease: a study of participants enrolled in an international sjogren's syndrome registry. *Arthritis Care Res (Hoboken)* (2012) 64(6):911–8. doi: 10.1002/acr.21610

4. Hernandez-Molina G, Kostov B, Brito-Zeron P, Vissink A, Mandl T, Hinrichs AC, et al. Characterization and outcomes of 414 patients with primary SS who developed hematological malignancies. *Rheumatol (Oxford)* (2022), keac205. doi: 10.1093/rheumatology/keac205

5. Thalayasingam N, Baldwin K, Judd C, Ng WF. New developments in sjogren's syndrome. *Rheumatol (Oxford)* (2021) 60(Suppl 6):vi53–61. doi: 10.1093/rheumatology/keab466

6. Kiripolsky J, Kramer JM. Current and emerging evidence for toll-like receptor activation in sjogren's syndrome. *J Immunol Res* (2018) 2018:1246818. doi: 10.1155/2018/1246818

7. Kiripolsky J, Kasperek EM, Zhu C, Li QZ, Wang J, Yu G, et al. Tissue-specific activation of Myd88-dependent pathways governs disease severity in primary sjogren's syndrome. *J Autoimmun* (2021) 118:102608. doi: 10.1016/j.jaut.2021.102608

8. Kiripolsky J, McCabe LG, Gaile DP, Kramer JM. Myd88 is required for disease development in a primary sjogren's syndrome mouse model. *J leukocyte Biol* (2017) 102(6):1411–20. doi: 10.1189/jlb.3A0717-311R

9. Rahmani F, Rezaei N. Therapeutic targeting of toll-like receptors: a review of toll-like receptors and their signaling pathways in psoriasis. *Expert Rev Clin Immunol* (2016) 12(12):1289–98. doi: 10.1080/1744666X.2016.1204232

10. Elshabrawy HA, Essani AE, Szekanecz Z, Fox DA, Shahrara S. TLRs, future potential therapeutic targets for RA. *Autoimmun Rev* (2017) 16(2):103–13. doi: 10.1016/j.autrev.2016.12.003

11. Debreceni IL, Chimenti MS, Serreze DV, Geurts AM, Chen YG, Lieberman SM. Toll-like receptor 7 is required for lacrimal gland autoimmunity and type 1 diabetes development in Male nonobese diabetic mice. *Int J Mol Sci* (2020) 21 (24):9478. doi: 10.3390/ijms21249478

12. Brown GJ, Canete PF, Wang H, Medhavy A, Bones J, Roco JA, et al. TLR7 gain-of-function genetic variation causes human lupus. *Nature* (2022) 605 (7909):349–56. doi: 10.1038/s41586-022-04642-z

13. Foulquier N, Le Dantec C, Bettacchioli E, Jamin C, Alarcon-Riquelme ME, Pers JO. Machine learning for the identification of a common signature for Anti-SSA/Ro 60 antibody expression across autoimmune diseases. *Arthritis Rheumatol* (2022) 74(10):1706-1719. doi: 10.1002/art.42243

14. Imgenberg-Kreuz J, Almlof JC, Leonard D, Sjowall C, Syvanen AC, Ronnblom L, et al. Shared and unique patterns of DNA methylation in systemic lupus erythematosus and primary sjogren's syndrome. *Front Immunol* (2019) 10:1686. doi: 10.3389/fimmu.2019.01686

15. Rasmussen A, Radfar L, Lewis D, Grundahl K, Stone DU, Kaufman CE, et al. Previous diagnosis of sjogren's syndrome as rheumatoid arthritis or systemic lupus erythematosus. *Rheumatol (Oxford)* (2016) 55(7):1195–201. doi: 10.1093/rheumatology/kew023

16. Lee CT, Strek ME. The other connective tissue disease-associated interstitial lung diseases: Sjogren's syndrome, mixed connective tissue disease, and systemic lupus erythematosus. *Curr Opin Pulm Med* (2021) 27(5):388–95. doi: 10.1097/MCP.0000000000000791

17. Satterthwaite AB. TLR7 signaling in lupus b cells: New insights into synergizing factors and downstream signals. *Curr Rheumatol Rep* (2021) 23 (11):80. doi: 10.1007/s11926-021-01047-1

18. Fillatreau S, Manfroi B, Dorner T. Toll-like receptor signalling in b cells during systemic lupus erythematosus. *Nat Rev Rheumatol* (2021) 17(2):98–108. doi: 10.1038/s41584-020-00544-4

19. Chodisetti SB, Fike AJ, Domeier PP, Choi NM, Soni C, Rahman ZSM. TLR7 negatively regulates B10 cells predominantly in an IFNgamma signaling dependent manner. *Front Immunol* (2020) 11:1632. doi: 10.3389/fimmu.2020.01632

20. Soni C, Wong EB, Domeier PP, Khan TN, Satoh T, Akira S, et al. B cell-intrinsic TLR7 signaling is essential for the development of spontaneous germinal centers. *J Immunol* (2014) 193(9):4400–14. doi: 10.4049/jimmunol.1401720

21. Uematsu S, Akira S. Toll-like receptors and type I interferons. *J Biol Chem* (2007) 282(21):15319–23. doi: 10.1074/jbc.R700009200

22. Lau CM, Broughton C, Tabor AS, Akira S, Flavell RA, Mamula MJ, et al. RNA-Associated autoantigens activate b cells by combined b cell antigen receptor/Toll-like receptor 7 engagement. *J Exp Med* (2005) 202(9):1171–7. doi: 10.1084/jem.20050630

23. Christensen SR, Shlomchik MJ. Regulation of lupus-related autoantibody production and clinical disease by toll-like receptors. *Semin Immunol* (2007) 19 (1):11–23. doi: 10.1016/j.smim.2006.12.005

24. Negishi H, Endo N, Nakajima Y, Nishiyama T, Tabunoki Y, Nishio J, et al. Identification of U11snRNA as an endogenous agonist of TLR7-mediated immune pathogenesis. *Proc Natl Acad Sci U.S.A.* (2019) 116(47):23653–61. doi: 10.1073/pnas.1915326116

25. Ittah M, Miceli-Richard C, Gottenberg JE, Sellam J, Eid P, Lebon P, et al. Viruses induce high expression of BAFF by salivary gland epithelial cells through TLR- and type-I IFN-dependent and -independent pathways. *Eur J Immunol* (2008) 38(4):1058–64. doi: 10.1002/eji.200738013

26. Maria NI, Steenwijk E C, IJpma AS, van Helden-Meeuwsen CG, Vogelsang P, Beumer W, et al. Contrasting expression pattern of RNA-sensing receptors TLR7, RIG-I and MDA5 in interferon-positive and interferon-negative patients with primary sjogren's syndrome. *Ann Rheum Dis* (2017) 76(4):721–30. doi: 10.1136/annrheumdis-2016-209589

27. Shimizu T, Nakamura H, Takatani A, Umeda M, Horai Y, Kurushima S, et al. Activation of toll-like receptor 7 signaling in labial salivary glands of primary sjogren's syndrome patients. *Clin Exp Immunol* (2019) 196(1):39–51. doi: 10.1111/cei.13242

28. Zheng L, Zhang Z, Yu C, Yang C. Expression of toll-like receptors 7, 8, and 9 in primary sjögren's syndrome. *Oral Surg Oral Med Oral Pathol Oral Radiol Endod* (2010) 109(6):844–50. doi: 10.1016/j.tripleo.2010.01.006

29. Karlsen M, Jakobsen K, Jonsson R, Hammenfors D, Hansen T, Appel S. Expression of toll-like receptors in peripheral blood mononuclear cells of patients with primary sjogren's syndrome. *Scand J Immunol* (2017) 85(3):220–6. doi: 10.1111/sji.12520

30. Karlsen M, Jonsson R, Brun JG, Appel S, Hansen T. TLR-7 and -9 stimulation of peripheral blood b cells indicate altered TLR signalling in primary sjogren's syndrome patients by increased secretion of cytokines. *Scand J Immunol* (2015) 82(6):523–31. doi: 10.1111/sji.12368

31. Imgenberg-Kreuz J, Sandling JK, Bjork A, Nordlund J, Kvarnstrom M, Eloranta ML, et al. Transcription profiling of peripheral b cells in antibody-positive primary sjogren's syndrome reveals upregulated expression of CX3CR1 and a type I and type II interferon signature. *Scand J Immunol* (2018) 87(5):e12662. doi: 10.1111/sji.12662

32. Brauner S, Folkersen L, Kvarnstrom M, Meisgen S, Petersen S, Franzen-Malmros M, et al. H1N1 vaccination in sjogren's syndrome triggers polyclonal b cell activation and promotes autoantibody production. *Ann Rheum Dis* (2017) 76 (10):1755–63. doi: 10.1136/annrheumdis-2016-210509

33. Davies R, Sarkar I, Hammenfors D, Bergum B, Vogelsang P, Solberg SM, et al. Single cell based phosphorylation profiling identifies alterations in toll-like receptor 7 and 9 signaling in patients with primary sjogren's syndrome. *Front Immunol* (2019) 10:281. doi: 10.3389/fimmu.2019.00281

34. Wang Y, Roussel-Queval A, Chasson L, Hanna Kazazian N, Marcadet L, Nezos A, et al. TLR7 signaling drives the development of sjogren's syndrome. *Front Immunol* (2021) 12:676010. doi: 10.3389/fimmu.2021.676010

35. Witas R, Shen Y, Nguyen CQ. Bone marrow-derived macrophages from a murine model of sjogren's syndrome demonstrate an aberrant, inflammatory response to apoptotic cells. *Sci Rep* (2022) 12(1):8593. doi: 10.1038/s41598-022-12608-4

36. Demaria O, Pagni PP, Traub S, de Gassart A, Branzk N, Murphy AJ, et al. TLR8 deficiency leads to autoimmunity in mice. *J Clin Invest* (2010) 120(10):3651–62. doi: 10.1172/JCI42081

37. Allushi B, Bagavant H, Papinska J, Deshmukh US. Hyperglycemia and salivary gland dysfunction in the non-obese diabetic mouse: Caveats for preclinical studies in sjogren's syndrome. *Sci Rep* (2019) 9(1):17969. doi: 10.1038/s41598-019-54410-9

38. Hwang SH, Park JS, Yang S, Jung KA, Choi J, Kwok SK, et al. Metabolic abnormalities exacerbate sjogren's syndrome by and is associated with increased the population of interleukin-17-producing cells in NOD/ShiLtJ mice. *J Transl Med* (2020) 18(1):186. doi: 10.1186/s12967-020-02343-7

39. Kiripolsky J, Shen L, Liang Y, Li A, Suresh L, Lian Y, et al. Systemic manifestations of primary sjogren's syndrome in the NOD.B10Sn-*H2*^{b}/J mouse model. *Clin Immunol* (2017) 183:225–32. doi: 10.1016/j.clim.2017.04.009

40. Chodisetti SB, Fike AJ, Domeier PP, Singh H, Choi NM, Corradetti C, et al. Type II but not type I IFN signaling is indispensable for TLR7-promoted development of autoreactive b cells and systemic autoimmunity. *J Immunol* (2020) 204(4):796–809. doi: 10.4049/jimmunol.1901175

41. Chan EK, Damoiseaux J, Carballo OG, Conrad K, de Melo Cruvinel W, Francescantonio PL, et al. Report of the first international consensus on standardized nomenclature of antinuclear antibody HEp-2 cell patterns 2014-2015. *Front Immunol-* (2015) 6:412. doi: 10.3389/fimmu.2015.00412

42. Rasband WS. *ImageJ*. Bethesda, Maryland, USA: U.S. National Institutes of Health (1997-2016). Available at: http://imagej.nih.gov/ij/.

43. Schindelin J, Arganda-Carreras I, Frise E, Kaynig V, Longair M, Pietzsch T, et al. Fiji: an open-source platform for biological-image analysis. *Nat Methods* (2012) 9(7):676–82. doi: 10.1038/nmeth.2019

44. Schindelin J, Rueden CT, Hiner MC, Eliceiri KW. The ImageJ ecosystem: An open platform for biomedical image analysis. *Mol Reprod Dev* (2015) 82(7-8):518–29. doi: 10.1002/mrd.22489

45. Benjamini Y, Hochberg Y. Controlling the false discovery rate: a practical and powerful approach to multiple testing. *J R Stat Soc Ser B* (1995) 57:289–300. doi: 10.1111/j.2517-6161.1995.tb02031.x

46. Benjamini Y, Yekutieli D. The control of the false discovery rate in multiple testing under dependency. *Ann Stat* (2001) 29(4):1165–88. doi: 10.1214/aos/1013699998

47. R Core Team. *R: A language and environment for statistical computing.: R foundation for statistical computing* (2020). Vienna, Austria: R Foundation for Statistical Computing. Available at: https://www.R-project.org/ (Accessed August 22, 2022).

48. Daniels TE, Cox D, Shiboski CH, Schiodt M, Wu A, Lanfranchi H, et al. Associations between salivary gland histopathologic diagnoses and phenotypic features of sjogren's syndrome among 1,726 registry participants. *Arthritis Rheum* (2011) 63(7):2021–30. doi: 10.1002/art.30381

49. Sumida T, Iizuka M, Asashima H, Tsuboi H, Matsumoto I. Pathogenic role of anti-M3 muscarinic acetylcholine receptor immune response in sjogren's syndrome. *Presse Med* (2012) 41(9 Pt 2):e461–6. doi: 10.1016/j.lpm.2012.05.019

50. He J, Qiang L, Ding Y, Wei P, Li YN, Hua H, et al. The role of muscarinic acetylcholine receptor type 3 polypeptide (M3RP205-220) antibody in the saliva of patients with primary sjogren's syndrome. *Clin Exp Rheumatol* (2012) 30(3):322–6.

51. Okuma A, Hoshino K, Ohba T, Fukushi S, Aiba S, Akira S, et al. Enhanced apoptosis by disruption of the STAT3-IkappaB-zeta signaling pathway in epithelial cells induces sjogren's syndrome-like autoimmune disease. *Immunity* (2013) 38 (3):450–60. doi: 10.1016/j.immuni.2012.11.016

52. Kiripolsky J, Romano RA, Kasperek EM, Yu G, Kramer JM. Activation of Myd88-dependent TLRs mediates local and systemic inflammation in a mouse model of primary sjogren's syndrome. *Front Immunol* (2019) 10:2963. doi: 10.3389/fimmu.2019.02963

53. Papinska J, Bagavant H, Gmyrek GB, Sroka M, Tummala S, Fitzgerald KA, et al. Activation of stimulator of interferon genes (STING) and sjogren syndrome. *J Dent Res* (2018) 97(8):893–900. doi: 10.1177/0022034518760855

54. Papinska J, Bagavant H, Gmyrek GB, Deshmukh US. Pulmonary involvement in a mouse model of sjogren's syndrome induced by STING activation. *Int J Mol Sci* (2020) 21(12):5412. doi: 10.3390/ijms21124512

55. Shimizu T, Nakamura H, Kawakami A. Role of the innate immunity signaling pathway in the pathogenesis of sjogren's syndrome. *Int J Mol Sci* (2021) 22(6):3090. doi: 10.3390/ijms22063090

56. Rubtsova K, Rubtsov AV, Thurman JM, Mennona JM, Kappler JW, Marrack P. B cells expressing the transcription factor T-bet drive lupus-like autoimmunity. *J Clin Invest* (2017) 127(4):1392–404. doi: 10.1172/JCI91250

57. Rubtsov AV, Rubtsova K, Kappler JW, Marrack P. TLR7 drives accumulation of ABCs and autoantibody production in autoimmune-prone mice. *Immunol Res* (2013) 55(1-3):210–6. doi: 10.1007/s12026-012-8365-8

58. Rubtsov AV, Rubtsova K, Fischer A, Meehan RT, Gillis JZ, Kappler JW, et al. Toll-like receptor 7 (TLR7)-driven accumulation of a novel CD11c(+) b-cell population is important for the development of autoimmunity. *Blood* (2011) 118 (5):1305–15. doi: 10.1182/blood-2011-01-331462

59. Phalke S, Rivera-Correa J, Jenkins D, Flores Castro D, Giannopoulou E, Pernis AB. Molecular mechanisms controlling age-associated b cells in autoimmunity. *Immunol Rev* (2022) 307(1):79–100. doi: 10.1111/imr.13068

60. Zhang W, Zhang H, Liu S, Xia F, Kang Z, Zhang Y, et al. Excessive CD11c (+)Tbet(+) b cells promote aberrant TFH differentiation and affinity-based germinal center selection in lupus. *Proc Natl Acad Sci U.S.A.* (2019) 116 (37):18550–60. doi: 10.1073/pnas.1901340116

61. Glauzy S, Boccitto M, Bannock JM, Delmotte FR, Saadoun D, Cacoub P, et al. Accumulation of antigen-driven lymphoproliferations in complement receptor 2/CD21(-/low) b cells from patients with sjogren's syndrome. *Arthritis Rheumatol* (2018) 70(2):298–307. doi: 10.1002/art.40352

62. Saadoun D, Terrier B, Bannock J, Vazquez T, Massad C, Kang I, et al. Expansion of autoreactive unresponsive CD21-/low b cells in sjogren's syndrome-associated lymphoproliferation. *Arthritis Rheum* (2013) 65(4):1085–96. doi: 10.1002/art.37828

63. Rubtsov AV, Rubtsova K, Kappler JW, Jacobelli J, Friedman RS, Marrack P. CD11c-expressing b cells are located at the T Cell/B cell border in spleen and are potent APCs. *J Immunol* (2015) 195(1):71–9. doi: 10.4049/jimmunol.1500055

64. Hao Y, O'Neill P, Naradikian MS, Scholz JL, Cancro MP. A b-cell subset uniquely responsive to innate stimuli accumulates in aged mice. *Blood* (2011) 118 (5):1294–304. doi: 10.1182/blood-2011-01-330530

65. Reincke ME, Payne KJ, Harder I, Strohmeier V, Voll RE, Warnatz K, et al. The antigen presenting potential of CD21(low) b cells. *Front Immunol* (2020) 11:535784. doi: 10.3389/fimmu.2020.535784

66. Keller B, Strohmeier V, Harder I, Unger S, Payne KJ, Andrieux G, et al. The expansion of human T-bet(high)CD21(low) b cells is T cell dependent. *Sci Immunol* (2021) 6(64):eabh0891. doi: 10.1126/sciimmunol.abh0891

67. Syrett CM, Anguera MC. When the balance is broken: X-linked gene dosage from two X chromosomes and female-biased autoimmunity. *J leukocyte Biol* (2019) 106(4):919–32. doi: 10.1002/JLB.6RI0319-094R

68. Ricker E, Manni M, Flores-Castro D, Jenkins D, Gupta S, Rivera-Correa J, et al. Altered function and differentiation of age-associated b cells contribute to the female bias in lupus mice. *Nat Commun* (2021) 12(1):4813. doi: 10.1038/s41467-021-25102-8

69. Christensen SR, Shupe J, Nickerson K, Kashgarian M, Flavell RA, Shlomchik MJ. Toll-like receptor 7 and TLR9 dictate autoantibody specificity and have opposing inflammatory and regulatory roles in a murine model of lupus. *Immunity* (2006) 25(3):417–28. doi: 10.1016/j.immuni.2006.07.013

70. Deane JA, Pisitkun P, Barrett RS, Feigenbaum L, Town T, Ward JM, et al. Control of toll-like receptor 7 expression is essential to restrict autoimmunity and dendritic cell proliferation. *Immunity* (2007) 27(5):801–10. doi: 10.1016/j.immuni.2007.09.009

71. Fayyaz A, Kurien BT, Scofield RH. Autoantibodies in sjogren's syndrome. *Rheum Dis Clin North Am* (2016) 42(3):419–34. doi: 10.1016/j.rdc.2016.03.002

72. Yaniv G, Twig G, Shor DB, Furer A, Sherer Y, Mozes O, et al. A volcanic explosion of autoantibodies in systemic lupus erythematosus: a diversity of 180 different antibodies found in SLE patients. *Autoimmun Rev* (2015) 14(1):75–9. doi: 10.1016/j.autrev.2014.10.003

73. Ching KH, Burbelo PD, Tipton C, Wei C, Petri M, Sanz I, et al. Two major autoantibody clusters in systemic lupus erythematosus. *PloS One* (2012) 7(2): e32001. doi: 10.1371/journal.pone.0032001

74. Kelly KM, Zhuang H, Nacionales DC, Scumpia PO, Lyons R, Akaogi J, et al. "Endogenous adjuvant" activity of the RNA components of lupus autoantigens Sm/RNP and ro 60. *Arthritis Rheum* (2006) 54(5):1557–67. doi: 10.1002/art.21819

75. Han S, Zhuang H, Shumyak S, Yang L, Reeves WH. Mechanisms of autoantibody production in systemic lupus erythematosus. *Front Immunol* (2015) 6:228. doi: 10.3389/fimmu.2015.00228